Comparison of Stereo-Extracted DTM from Different High-Resolution Sensors: SPOT-5, EROS-A, IKONOS-II, and QuickBird♥

Thierry Toutin
Canada Centre for Remote Sensing, Natural Resources Canada
588, Booth Street, Ottawa, Ontario K1A 0Y7

Abstract- Digital elevation models (DEMs) extracted from high-resolution stereo images (SPOT-5, EROS-A, IKONOS-II and QuickBird) using a three-dimensional multisensor physical model developed at the Canada Centre for Remote Sensing, Natural Resources Canada were evaluated. In a first step, the photogrammetric bundle adjustment was setup for the stereo-images with few accurate ground control points. In a second step, DEMs were generated using an area-based multiscale image matching method and then compared to 0.2-m accurate light detection and ranging (LIDAR) elevation data. Elevation linear errors with 68% confidence level (LE68) of 6.5, 20, 6.4, and 6.7 m were achieved for SPOT, EROS, IKONOS and QuickBird, respectively. The poor results for EROS are mainly due to its asynchronous low orbit, which generated large geometric and radiometric differences. However, when such differences were not large, LE68 of 10 m (four pixels) was achieved. Since the SPOT, IKONOS and QuickBird DEMs were in fact digital surface models, where the height of land covers was included, elevation accuracy was performed only on bare surfaces (soils and lakes), where there was also no difference between the stereo-extracted elevations and the LIDAR data. LE68 of 2.2, 1.5, and 1.2 m were then obtained for SPOT, IKONOS and QuickBird, respectively. When compared to sensor resolution, multidate across-track SPOT, with a smaller base-to-height (*B/H*) ratio of 0.77**,** achieved three to four times better results than same-date in-track IKONOS and QuickBird with *B/H* of around one: 0.5 pixel versus 1.5 or 2 pixels.

Index Terms- Digital elevation model (DEM), geometric evaluation, high resolution, stereoscopy.

I INTRODUCTION

The generation of high-resolution (HR) imagery using previously proven defence technology provides an interesting source of data for digital topographic mapping as well as thematic applications such as agriculture, forestry, and emergency response [1], [2]. Technical information regarding U.S. civilian satellites with their applicability to Earth sciences have been summarized in [3]. Since the launch of IKONOS-II with HR sensors (1-m panchromatic, Pan and 4-m multiband, XS) on September 24, 1999, other pushbroom satellite scanners such as Earth Resources Observation System A (EROS-A), QuickBird, Système Pour l'Observation de la Terre 5 (SPOT-5), and OrbView, are now available with resolutions of 0.61 m (QuickBird) to 5 m (SPOT). Most (EROS,

♥ Published in IEEE-TGARS, 42(10):2121-2129, 2004

IKONOS, OrbView, and QuickBird) are agile satellites (off-nadir viewing capability up to 60º in any azimuth), while SPOT-5, with its high-resolution-geometry (HRG) sensors, kept its traditional multidate across-track viewing capability [4]. The agile pointing capability enables the generation of same-date in-track stereoscopy from the same orbit, which has a stronger advantage to multidate across-track stereo-data acquisition because it reduces radiometric image variations, (temporal changes, sun illumination, etc.), and thus increases the correlation success rate in any image matching process [5]. Both acquisition methods can generate strong stereo geometry with base-to-height ratio (*B/H*) of one, and users can apply traditional three-dimensional (3-D) photogrammetric techniques with the stereo-images to extract accurate planimetric and elevation information.

Due to the high spatial resolution of recent airborne/spaceborne sensors in the visible and micro-wave spectrum, a large number of researchers around the world have investigated the extraction of elevation and/or the production of digital elevation models (DEMs) using different methods [5]–[7]. In preparation for the launch of HR civilian satellites it was demonstrated using similar systems mounted on aircraft platforms or from scanned aerial photos that IKONOS stereo-images should have the potential of creating DEMs with an accuracy of about 2 m [8], but only if photogrammetric processing was employed [9]. Later on, some studies generated a full DEM from IKONOS stereo-images using an automatic process [10]–[12]. The objectives of this paper are to evaluate and to compare, with accurate LIDAR ground truth, DEMs generated from different HR sensors (resolutions of 0.61–5 m, in-track versus across-track stereo-acquisitions) using a photogrammetric-based 3-D multisensor physical geometric model developed at the Canada Centre for Remote Sensing (CCRS), Natural Resources Canada [13], [14].

II DESCRIPTION OF THE METHOD

A. Study Site and High-Resolution Stereo Data

The study site is an area north of Québec City, Qc, Canada (N 47º, W 71º 30') (Fig. 1). This study area consists of an urban/residential environment in the southern part and is covered 80% by forests (deciduous, conifer and mixed) in the northern part. The site has a hilly topography, with an elevation range of more than 1000 m from sea level at the St. Lawrence River, located to the southeast, to the mountains in the north, and a mean slope of 10º. Four HR stereo-images were acquired in panchromatic mode over this study site: SPOT-5 (5 m, *B/H* of 0.77), EROS-A (1.8 m, *B/H* of 0.7), IKONOS-II (0.8 m, *B/H* of 1) and QuickBird (0.61 m, *B/H* of 1.1) (Table I). Most of the images were acquired during the wintertime (January to May) with snow and ice present, and with low sun illumination angles, 24° and 19° for EROS (Fig. 2) and IKONOS (Fig. 3) respectively, which resulted in long shadows. On the other hand, QuickBird data acquired on April 1, 2003 displays few shadows due only to vertical structures, but snow in most of the bare surfaces (Fig. 4): sand/gravel pits, frozen lakes, power-line

corridors, and downhill ski tracks. Nevertheless, snow and ice are less problematic with same-date stereo-pair than with multidate stereo-pair. SPOT data acquired on May 5, 2003 (Fig. 1) displays snow in the forests (upper part) and frozen lakes (lower left and center), for almost 50% of the image, but not the May 25 image. These differences in snow/ice generated large radiometric differences in SPOT stereo-images. However, these differences provide an opportunity to test DEM generation method and address potential problems in difficult conditions instead of working in a perfect environment.

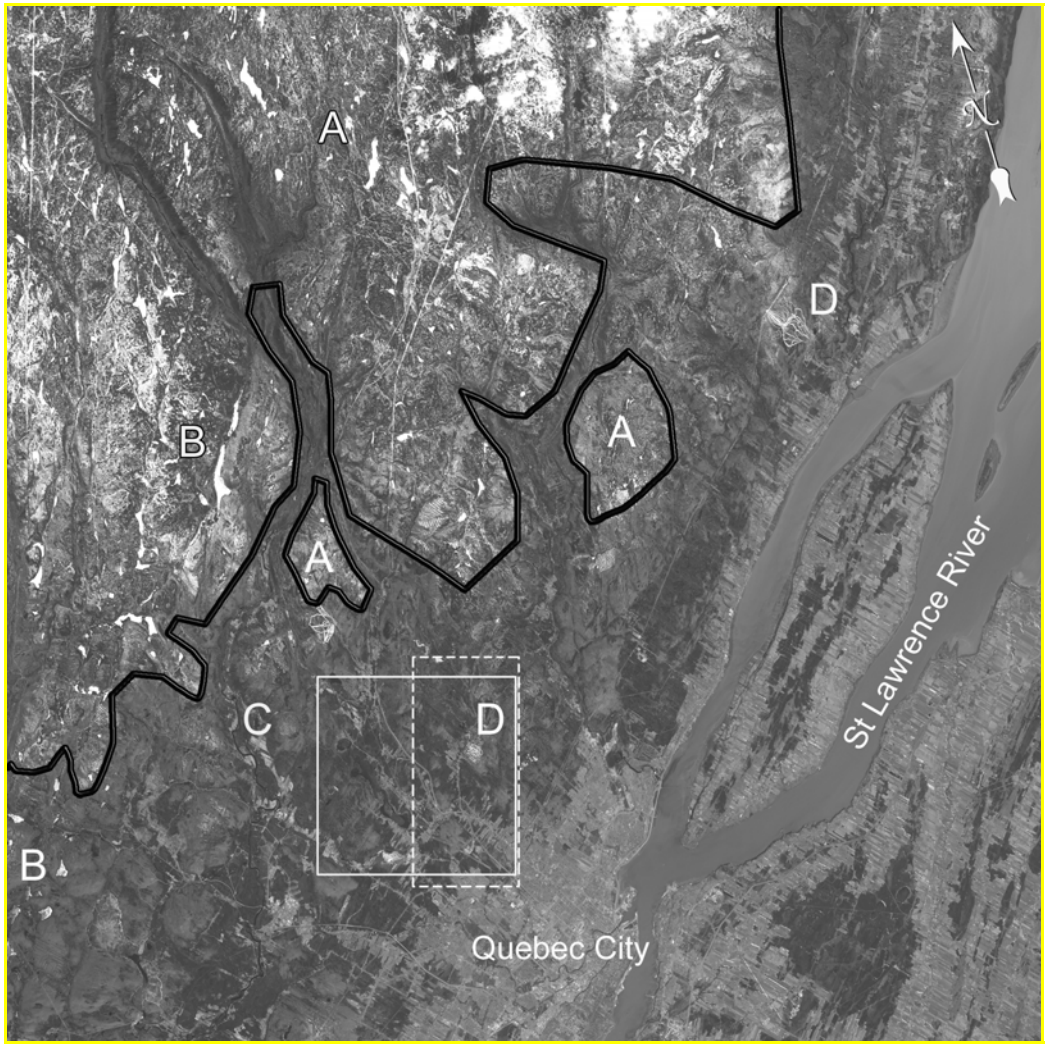

Figure 1. SPOT-5 HRG image (May 5 2003; 23° west-viewing angle; 60 km × 60 km; 5-m pixel spacing) displaying the study site. Québec city is on the center-south and the river is the St. Lawrence River. The white square approximately represents the EROS, IKONOS and QuickBird image location, and the dashed-line rectangle represents the LIDAR acquisition location. Note: (A) the melting snow in the half-north of the image; (B) frozen lakes; (C) lakes with significant melting ice; (D) down-hill ski stations with snow.
SPOT Image © CNES, 2003; Courtesy of SPOT-IMAGE.

Table I: Characteristics of the four stereo-pairs acquired over the study site, Québec, Canada.

Stereo-pair	Acquisition Date	Sun angle	Stereo	View angles	Image (km)	Pixel (m)	Nb. GCPs
SPOT-5 HRG	May 05, 2003 May 25, 2003	52º 55º	Multidate Across	+ 23º -19º	60 x 60	5 x 5	33
EROS-A Pan	February 6, 2002	24º	Same date Along	+ 30º-8º - 6º-27º	13 x 13	1.8 to 2.4	130
IKONOS-II Pan	January 3, 2001	19º	Same date Along	±27º	10 x 10	1 x 1	55
QuickBird Pan	April 1, 2003	45º	Same date Along	±29º	18 x 15	0.61 x 0.61	48

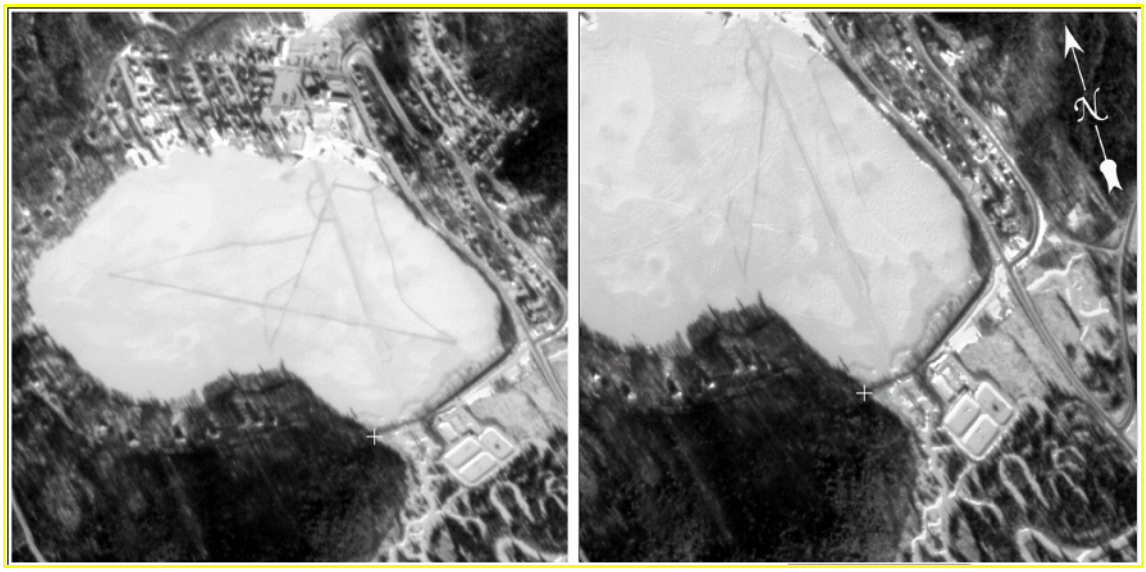

Figure 2. Subimage of the EROS-A stereo pair (512 × 512 pixels) acquired over Québec, Canada. Note the shadows on the lake and the impact of attitude variations of the asynchronous EROS satellite, such as the shape and size variations of the lake, skidoo tracks, and roads. EROS Images © and courtesy ImageSat Intl., 2002.

SPOT, IKONOS and QuickBird are synchronous satellites [4], [15] while EROS satellites are asynchronous [16]. EROS is thus "too fast" and must continuously pitch backward and yaw during the image acquisition[1] (Fig. 5). Since scanning angles change as the satellite "bends backward" during the scanning process, the imagery's shape is further distorted and the ground resolution continuously changes, even locally (Fig. 2). The SPOT and EROS images are raw level-1A data, orbit oriented, with detector

[1] http://www.imagesatintl.com/customersupport/techarticles/Tutorial_SatelliteImaging_Non-synchronousMode.pdf

equalization only. Ephemeris and attitude data are available in the metadata as well as general information related to the sensor and satellite. The IKONOS images are geometrically and radiometrically preprocessed and only distributed in a quasi-epipolar-geometry reference where just the elevation parallax in the scanner direction remains. For in-track stereoscopy with the IKONOS orbit, the image orientation corresponds approximately to a north-south direction, with few degrees in azimuth depending on the across-track component of the total collection angle (Fig. 3). Conversely to other satellites, few metadata on satellite and sensor geometry are available. The QuickBird images (Basic 1B product) are also geometrically and radiometrically preprocessed to simulate the imaging geometry of a simple pushbroom linear array. To realize this virtual ideal linear array imagery, the detector misalignments and the optical distortions are removed and the attitude jitter are corrected [17].

Figure 3. Subimage of backward image of the IKONOS-II stereo pair, north of Québec City, Québec, Canada. Note (A) tree shadows, (B) mountain shadows due to 19° solar elevation angle and 166° azimuth angle, and (C) a skater on the frozen lake.
IKONOS Image © Space Imaging LLC, 2001.

Figure 4. Forward QuickBird image (18 km × 15 km; 0.61-m pixel spacing), north of Québec, Canada acquired April 1, 2003. Note (A) sand/gravel pits, (B) snow-covered frozen lakes, (C) snow-covered bare soils, (D) power-line corridors, and (E) downhill ski tracks.
QuickBird Image © and Courtesy DigitalGlobe, 2003

Ground control points (GCPs) were collected in stereoscopy for the different tests on the bundle adjustment of the stereoscopic pairs. For SPOT and EROS, GCP cartographic coordinates (*X*, *Y, Z*) were obtained from 1:20,000 digital topographic maps provided by the *Ministère des Ressources naturelles du Québec*, Canada. The accuracy of these maps is estimated to be around 2 m in planimetry and 3 m in elevation. Because of the good resolution of the IKONOS and QuickBird sensor, GCP cartographic coordinates (*X*, *Y, Z*) were stereo-compiled using a Wild A-10 by the same *Ministère* from aero-triangulated 1:40 000 photos. GCP accuracy is estimated to be better than 1 m and 2 m in planimetry and elevation, respectively.

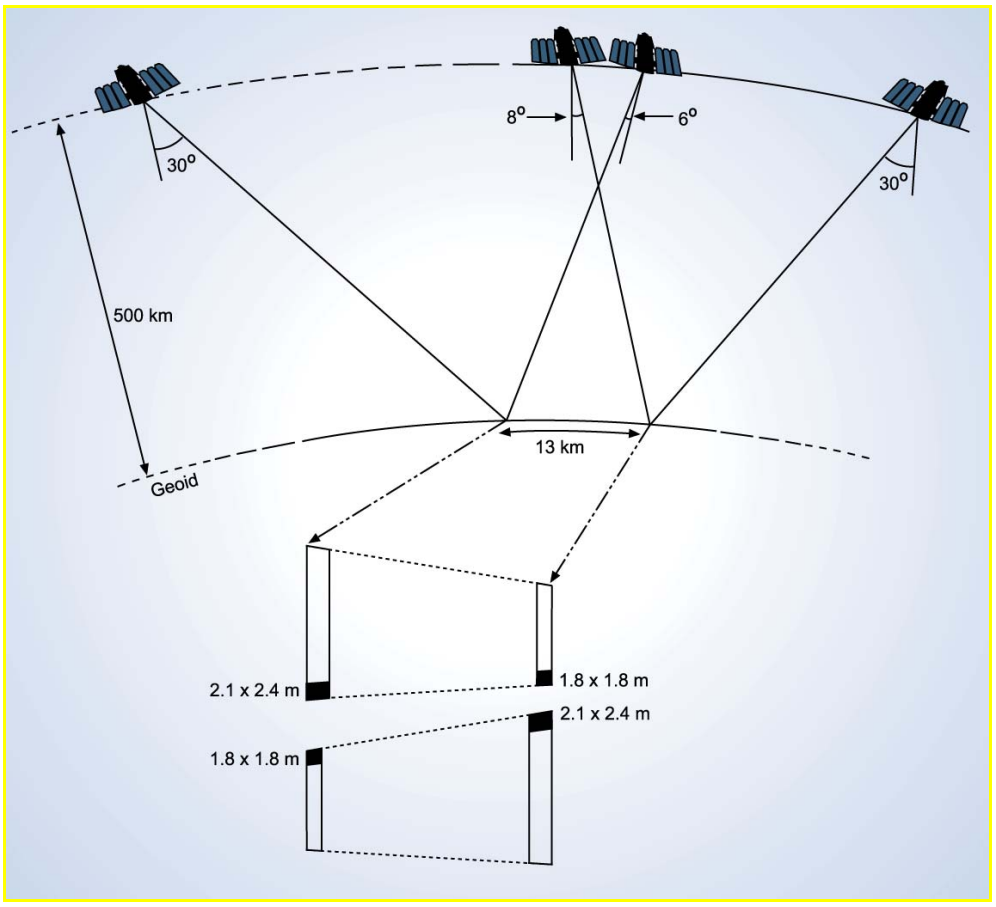

Figure 5. Examples of the pitch variations of our EROS-A stereo-data and its impact on the pixel spacing.

To evaluate the accuracy of the stereo-extracted DEMs, accurate spot elevation data was obtained from a LIDAR survey conducted by GPR Consultants (www.lasermap.com) on September 6, 2001. The Optech ALTM-1020 system is comprised of a high-frequency optical laser coupled with a Global Positioning System (GPS) and an Inertial Navigation System (INS)[2]. A 3-D GPS solution (*X*, *Y*, *Z*) is used to position the laser scanner at each second or half second, while the INS data are used to determine the system's orientation. The GPS solution is computed from differential kinematic processing, using data collected simultaneously at the aircraft, and at base stations near the project site [18]. From a fixed-wing airborne platform, the laser emits pulses at frequencies of up to 5000 Hertz and the first echoed pulses are reflected off vegetation or man-made structures and recorded. With 700–850-m flying height, 70-m/s velocity, 5000-Hz pulse rate, 12-Hz scanning frequency, and ±20° scan angle (510–630 m wide swath), the ground point density is about 300,000 3-D point/min, and the accuracy is

[2] www.optech.on.ca

0.30 m in planimetry and 0.15 m in elevation. Since it was impossible to cover the full SPOT coverage (60 km × 60 km), ten swaths covering an area of 5 km × 13 km (Fig. 1) and representative of the full study site were acquired. The results of the LIDAR survey are then an irregular-spacing grid (around 3 m), due also to no echo return in some conditions such as buildings with black roofs, roads, and lakes. Since the objectives of this research study were to evaluate the stereo DEMs, the LIDAR elevation data was not interpolated into a regular spacing grid so as to avoid the propagation of interpolation error into the checked elevation and evaluation.

B. Three-Dimensional CCRS Multisensor Physical Model

The 3-D CCRS multisensor physical model was originally developed to suit the geometry of pushbroom scanners, such as SPOT-HRV, and has been subsequently adapted as an integrated and unified geometric modeling to geometrically process multisensor images. More details on the mathematic model, development (colinearity equations) and its applicability to HR images can be found in [13] and [14]. In summary, the geometric modeling represents the well-known colinearity condition (and coplanarity condition for stereo-model) and takes into account the different distortions relative to the global geometry of viewing, such as:

- distortions relative to the platform (position, velocity, orientation);
- distortions relative to the sensor (orientation angles, instantaneous field of view, detection signal integration time);
- distortions relative to the Earth (geoid-ellipsoid including elevation); and
- deformations relative to the cartographic projection (ellipsoid-cartographic plane).

Each of the unknown parameters is in fact the combination of several correlated variables of the total viewing geometry (platform, sensor, Earth, cartographic projection), so that the number of unknown parameters has been reduced to an independent uncorrelated set. The unknown parameters are thus translations (in X and Y) and a rotation related to the cartographic north, the scale factors and the leveling angles in both directions, the non-perpendicularity of axes, as well as some second-order parameters when the orbital/attitude data are not known (IKONOS) or accurate (EROS).

This 3-D physical model has been applied to visible and infrared (VIR) data (MODIS, MERIS, Landsat-5/7, SPOT-1 to -5, IRS-1C/D, ASTER, Kompsat-1 EOC), HR VIR data (SPOT-5, EROS-A, IKONOS-II, OrbView, QuickBird and airborne data), as well as radar data (ERS-1/2, JERS, SIR-C, RADARSAT, ENVISAT and airborne data) with three to six GCPs. This model is robust and not sensitive to GCP distribution as soon as there is no extrapolation in planimetry and elevation [13], [14]. Based on good quality GCPs, the accuracy of this model is within one-third of a pixel for medium-resolution VIR images, sub-pixel for HR images and one resolution cell for radar images.

C. Processing Steps of DEM Generation

Since the processing steps of DEM generation from HR stereo images are roughly the same as for other stereo-images (data collection and preprocessing, stereo bundle adjustment with GCPs, elevation parallax measurements, DEM generation), the five processing steps are summarized:

Step 1) Acquisition and preprocessing of the remote sensing data (images and metadata) to determine an approximate value for each parameter of 3-D physical model for the two images.

Step 2) Collection of stereo GCPs with their 3-D cartographic coordinates and two-dimensional (2-D) image coordinates. GCPs covered the total surface with points at the lowest and highest elevation to avoid extrapolations, both in planimetry and elevation. The image pointing accuracy was around half-pixel for SPOT (2.5 m), more than one pixel for EROS (2 m) and one to two pixels for IKONOS and QuickBird (1–2 m).

Step 3) Computation of the 3-D stereo model, initialized with the approximate parameter values and refined by an iterative least squares bundle adjustment with the GCPs [Step 2)] and orbital constraints. Both equations of colinearity and coplanarity are used as observation equations and weighted as a function of input errors. All points, with fixed coordinates for GCPs, are weighted as a function of their accuracy (cartographic and image coordinates) to set up the normal equations, which were resolved with a conventional Cholesky's inversion process [19]. GCP residuals and Independent Check Points (ICPs) errors are the differences between the "true" cartographic coordinates and the computed cartographic coordinates. Theoretically four to seven accurate GCPs, depending upon the sensor, are enough to compute the stereo model. More GCPs were acquired so as to have an overestimation in the adjustment, to reduce the impact of input data errors (cartographic and image pointing) and to perform accuracy tests and evaluations with ICPs.

Step 4) Extraction of elevation parallaxes using multiscale (three steps) mean-normalized cross-correlation method with computation of the maximum of the correlation coefficient. This method gave good results and was commonly used with satellite images [20].

Step 5) Computation of *XYZ* cartographic coordinates from elevation parallaxes in a regular grid spacing [Step 4)] using the previously-computed stereo-model (Step 3) with 3-D least squares stereo-intersection.

After some blunder removal, the DEMs were evaluated with the LIDAR elevation data. About five to six millions of points, corresponding to the overlap area between the

stereo-pair and the LIDAR coverages (Fig. 1), were used in the statistical computation of elevation errors.

III RESULTS AND DISCUSSIONS

Error propagation can be tracked along the processing steps with stereo-bundle adjustment results [Step 3)], and during the DEM generation [Step 4) and Step 5)]. For these two last steps, qualitative results are given for each stereo-pair, but the quantitative results on DEMs are only given, where LIDAR elevation data (5 km × 13 km) was acquired (Fig. 1).

A. Stereo-Bundle Adjustment Results

As a function of the number of GCPs used in the stereo bundle adjustment, two sets of tests were performed for each stereo-pair. Set 1 was conducted with all the GCPs, while Set 2 was performed with a reduced number of GCPs (10–18) and the remaining points as ICPs. In Set 2, ten GCPs were used for SPOT, IKONOS, and QuickBird data because previous results demonstrated that this was a good compromise with this dataset to avoid the propagation of input data error (cartographic and mainly image pointing) into the 3-D physical stereo-models [13], [14]. More GCPs (18) were used with EROS data due to the increased number of unknown parameters, which physically model the largest attitude variations, in order to keep the same degree of freedom in the least squares adjustment. The remaining points as ICPs, which were not used in the 3-D stereo-model calculations, are used for performing unbiased validations of the modeling accuracy. Table II summarizes the results of the two sets: Set 1 with the residuals on GCPs (root mean square (RMS) and maximum) when all GCPs were used, and Set 2 with the RMS residuals and errors on GCPs and ICPs, respectively when 10–18 GCPs were used in the least squares adjustment of stereo-models.

Table II: Results of stereo-bundle adjustment for two different sets of tests: the number of GCPs and ICPs and the root mean square (RMS) residuals on GCPs (in meters) for both Sets with either the maximum residuals (in meters) on GCPs for Set 1 or the RMS errors (in meters) on ICPs for Set 2.

Set 1 of Stereo Bundle Tests	**Number of GCPs**	**Number of ICPs**	**RMS GCP Residuals (m)**				**Maximum Residuals (m)**			
			X	***Y***	***XY***	***Z***	***X***	***Y***	***XY***	***Z***
SPOT-5	33	0	2.6	3.1	4.0	3.3	5.4	7.6	9.9	7.5
EROS-A	130	0	3.4	3.6	4.9	4.6	9.3	9.0	12.9	12.5
IKONOS-II	55	0	1.9	1.7	2.5	2.2	5.2	3.5	6.3	6.1
QuickBird	48	0	1.0	1.1	1.5	0.9	3.3	2.4	4.1	3.2
Set 2 of Stereo Bundle Tests	**Number of GCPs**	**Number of ICPs**	**RMS GCP Residuals (m)**				**RMS ICP Errors (m)**			
			X	***Y***	***XY***	***Z***	***X***	***Y***	***XY***	***Z***
SPOT-5	10	23	1.5	1.4	2.1	1.3	2.6	2.2	3.4	2.9
EROS-A	18	112	2.4	2.8	3.7	3.8	4.2	4.2	5.9	5.9
IKONOS-II	10	45	1.2	1.6	2.0	1.9	2.4	2.1	3.2	3.0
QuickBird	10	38	0.6	0.7	0.9	0.4	1.5	1.6	2.2	1.4

Due to the large redundancy of equations in the adjustments of Set 1, the RMS *X*-*Y* residuals (around 2–4 m in Table II) are on the same order of magnitude as the input data errors, being a combination of image pointing error (0.5–2 pixels) and planimetric error (1 or 2 m) in addition to the propagation of *Z*-error (2 or 3 m) depending on the viewing and azimuth angles (Table I). On the other hand, the RMS *Z* residuals (from 1–5 m depending on the sensors, Table II) reflect approximately the image pointing errors (2.5 m for SPOT; 2–3 m for EROS; 1–2 m for IKONOS, and 1 m for QuickBird) combined with a *B/H* of 0.77, 0.7, 1, and 1.1, respectively. The analysis of the *X*-*Y* maximum residuals, which are generally around 2–3 the RMS residuals, demonstrates that the 3-D physical models are stable over the entire stereo-images without generating local errors. The use of overabundant GCPs in the least squares adjustment reduced or even cancelled the propagation of different input data errors (image pointing error of 1–2 pixels and cartographic error of 1–2 m) into the 3-D physical stereo-models, but conversely these input errors are reflected in the residuals. Consequently, it is "normal and safe" to obtain RMS residuals from the least squares adjustment in the same order of magnitude as the input data error; however, the modeling or internal accuracy is better (around one pixel or less) [5], [14].

As mentioned previously, Set 2 of the tests enabled unbiased validation of the positioning and restitution accuracy with independent check data, such as ICPs (Table II). The different RMS residuals on GCPs are 20% to 40% smaller than the RMS residuals resulting from Set 1 because fewer GCPs, and thus less equation redundancy, were used in the least squares adjustments. Conversely, RMS errors on ICPs range from 1.5–5 m and, when compared to sensor resolution, range from 0.5 pixel for SPOT to around two pixels for the three other sensors. The main reasons why SPOT achieved the best results, when compared to resolution, are the strongest stability of synchronous versus asynchronous satellites as well as its 820-km altitude (less orbital perturbations) versus the 500–600-km altitudes for the three others.

However, these RMS errors, which include the extraction error (image pointing error of 0.5 pixel for SPOT and one or two pixels for the three others) of ICP features, are only an estimation of the 3-D restitution accuracy of planimetric and elevation features. The internal accuracy of stereo-models is thus better, in the order of subpixel for SPOT, IKONOS and QuickBird and one pixel for EROS.

B. DEM Evaluation Results

The second result is the qualitative and visual evaluation of the full DEMs and the quantitative and statistical evaluation of the DEMs with the LIDAR data. Fig. 6 is the full DEM (60 km × 60 km; 5-m grid spacing) extracted from SPOT, which well reproduces the terrain relief and different features (see Fig. 1), such as mountains, valleys, the St. Lawrence River and a large island. Even some small relief features between the mountains and the St. Lawrence valley were captured. The black areas correspond to mismatched areas due to radiometric differences between the multidate

images, as a result of snow in the mountains and on frozen lakes (only on the May 5 image), as well as the St. Lawrence River. Fig. 7 is an example of the mismatched problems. The left part is a color composite of the two images where the red areas represent the radiometric differences due to snow and ice, and the superimposed yellow lines are the limits of mismatched areas. There is a strong correlation between the two areas, mainly at the downhill ski-tracks in the mountains and lakes. The right part of this Plate is an enlargement of the two images that clearly shows and explains the "mismatched" reasons: in the May 5 image (bottom-right), there is still snow in the mixed and sparse forests, as well as ice on the lake while in the May 25 image (top-right) these features have completely disappeared.

Figure 6. DEM (60 km × 60 km; 5 m spacing) extracted from the SPOT-5 stereo pair. The black areas correspond to mismatched due to radiometric differences between the multi-date images, as a result of (A) melting snow in the mountains, (B) frozen lakes and (C) the St. Lawrence River (see Fig. 1).

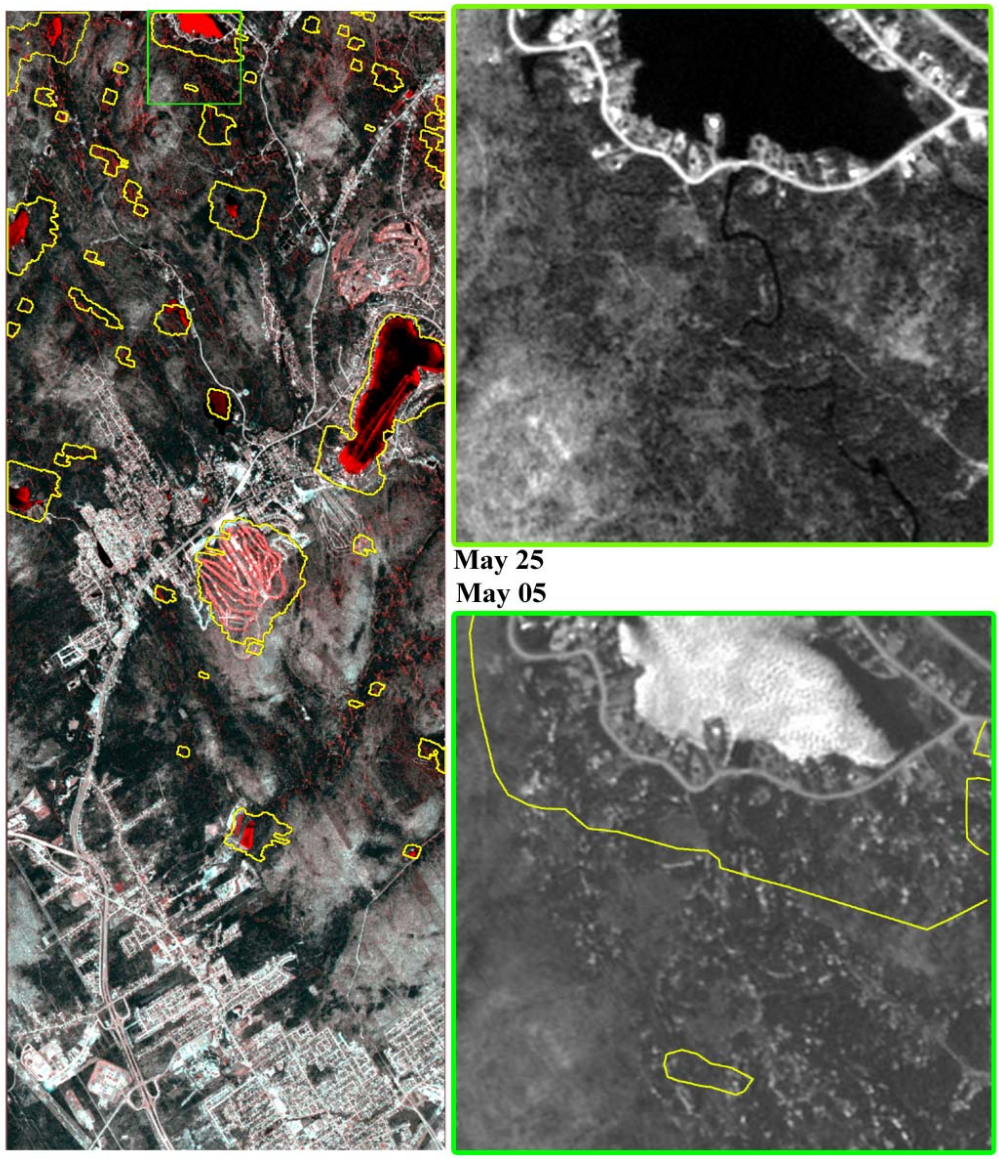

Figure 7. SPOT-5 HRG (May 25 and May 5, 2003) composite subimage (left) shows the radiometric differences (in red) correlated with the mismatched areas (in yellow). The feature in the center is a downhill ski station (D in Figure 1). The enlargement of the two images (May 25 top-right and May 5 bottom-right) shows and explains the "mismatched" reasons. In the May 5 image, there is still snow in the mixed and sparse forests, as well as ice on the lake while they are completely disappeared in the May 25 image. SPOT Images © CNES, 2003; Courtesy of SPOT-IMAGE.

Fig. 8 is the full DEM (13 km × 13 km; 2-m grid spacing) extracted from EROS, which reproduces the general features of the terrain relief, such as the small mountains in the center, but not the smallest details of relief. Even though the images were acquired in

February, the mismatched areas (in black), located mainly in the top of the stereo-pair are not due to snow cover and frozen lakes ("equivalent" features in the same-date in-track stereo-images) but rather to a combination of two other factors that generated uncertainty and errors in the matching process. These factors were the quite different pixel spacing (geometric factor) of both images (Figs. 2 and 5), and a lack of well defined features (radiometric factor) of the area covered by forest. When one of these factors was absent, the matching process performed well: either in the center of the stereo-pair where the image pixel sizes are more identical or in the bottom of the stereo-pair where well-defined features of residential areas enabled a good match.

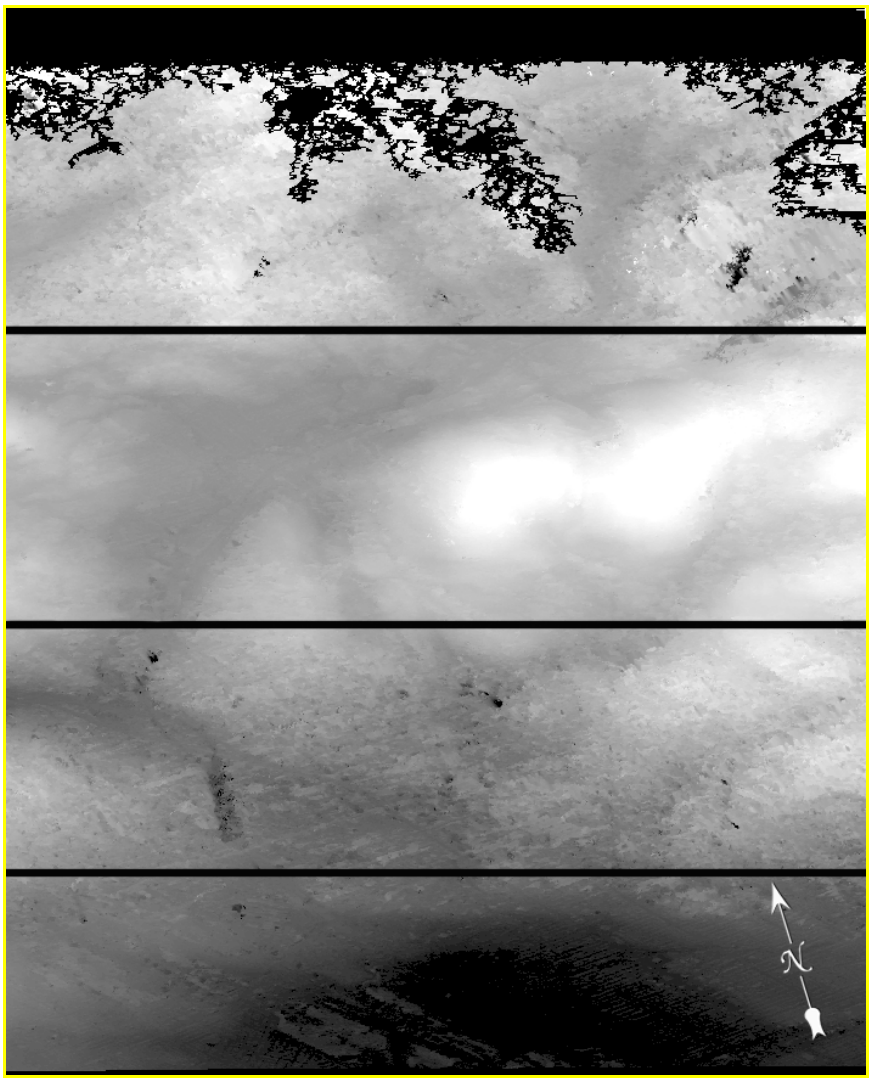

Figure 8. DEM (13 km × 13 km; 2-m spacing) extracted from the EROS-A stereo pair. Large mismatched areas occur in the top of the stereo-pair due to a combination of two factors: differences of pixels of the stereo-images and forest coverage. The DEM is cut into four horizontal parts according to the matching score results for the evaluation of the elevation accuracy.

Figs. 9 and 10 are the full DEMs (10 km × 10 km and 18 km × 15 km, respectively; 1-m pixel spacing) extracted from IKONOS and QuickBird respectively, which reproduce the full terrain relief better with higher topographic details and different cartographic features than the two previous DEMs. In addition, specific or small features visible on the IKONOS and QuickBird images are also identifiable on the DEMs due to elevation differences. These features include:

- In Fig. 9, sand/gravel pits in A; some patterns in B related to streets/houses in residential areas; linear features in C related to main roads, and power-line clearcut in the forest environment and lakes in D.

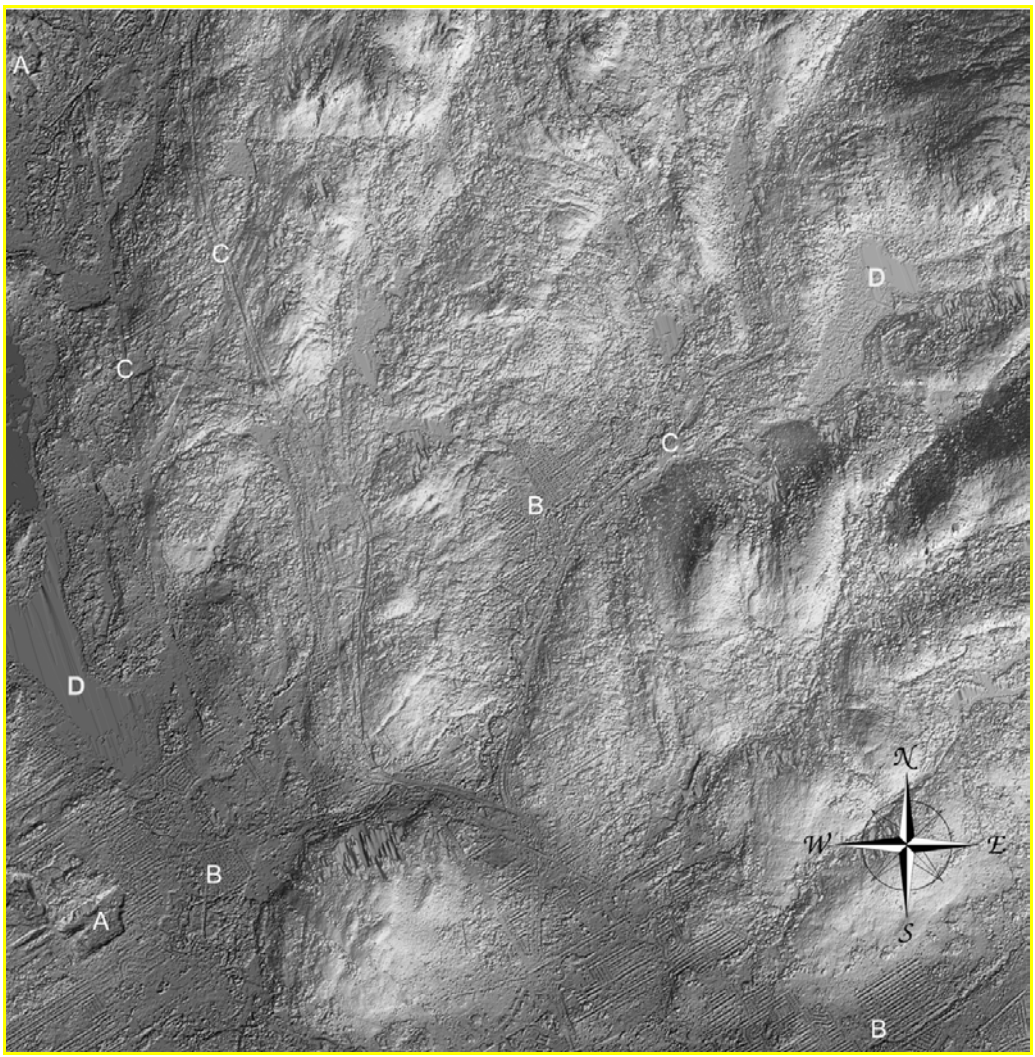

Figure 9. DEM (10 km × 10 km; 1 m spacing) extracted from the IKONOS-II stereo-pair. Noticeable cartographic features include: (A) sand pits, (B) residential areas, (C) roads and power lines, and (D) lakes. The linear features, which occur in residential areas (B), are not artefacts or systematic errors but are related to streets and houses patterns.

- In Fig. 10 with the shaded-relief subimages: sand/gravel pits in A; lakes in B; bare soils in C; power-line corridors in D; residential areas in E; deciduous and sparse trees without leaves in F, and highways in G.

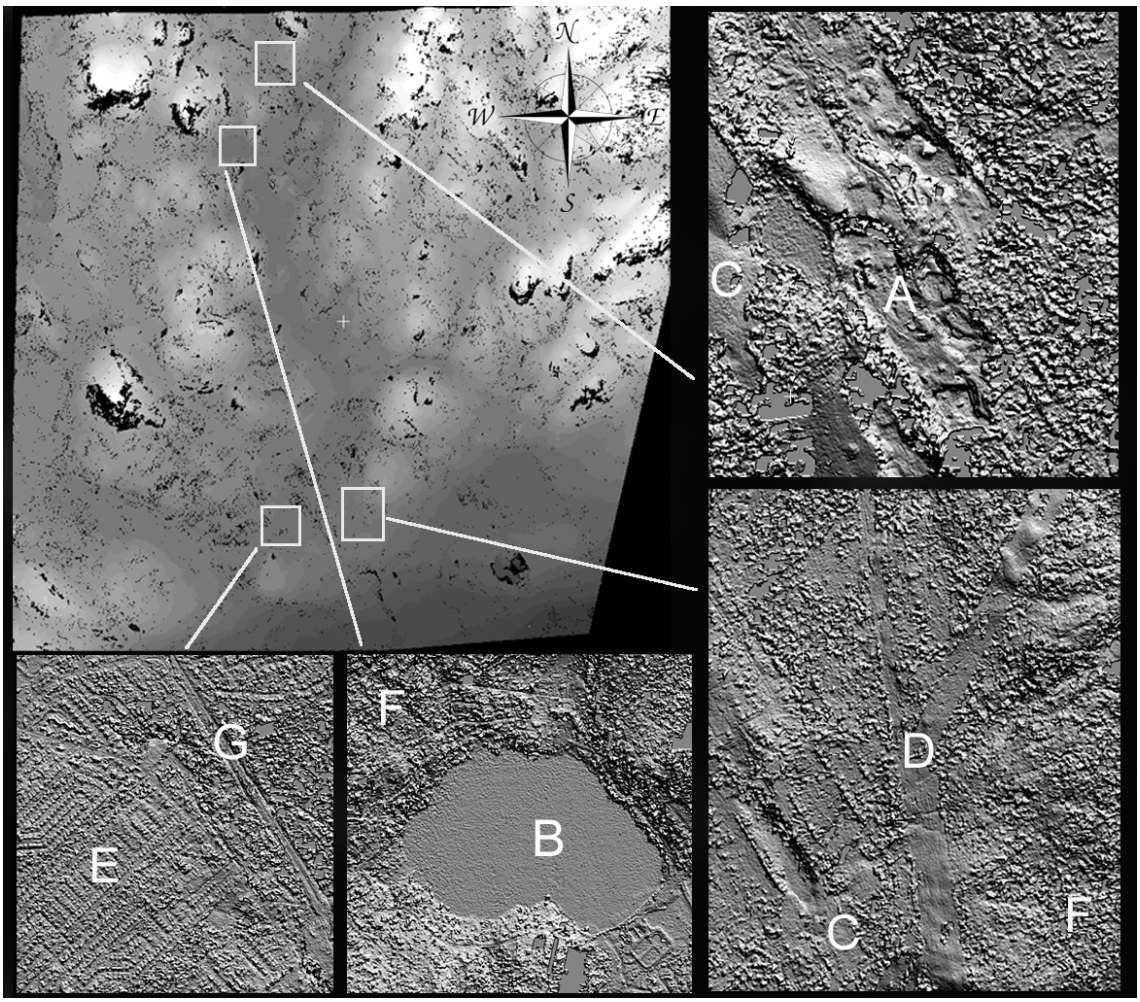

Figure 10. Stereo-extracted DEM (18 km × 15 km; 1-m pixel spacing) extracted from the QuickBird stereo-pair with shaded relief enhancement for some sub-areas. Black areas are the mismatched areas (6% of the total area). Note (A) sand/gravel pits, (B) lakes, (C) bare soils, (D) power-line corridors, (E) residential areas, (F) deciduous and sparse trees without leaves, and (G) highways.

Even though the images were acquired in January or April with snow cover and frozen lakes, there were only few mismatched areas (5% to 6 % of the total area). The first reason is the same-date in-track stereo-acquisition, which greatly reduces the temporal differences in radiometry. The second reason is the sensor resolution of less than 1 m: the blown ice/snow, the tracks of snowmobiles, skaters and others features created texture and contrast on snow-covered bare surfaces (Figs. 3 and 4). For IKONOS, some

mismatched areas were located in the northwest slopes of the mountains (Fig. 3) due to solar shadow (elevation angle of 19º and azimuth of 166º).

Quantitative evaluation of DEMs was conducted with the comparison of the LIDAR elevation data and five to six million elevation points were used in statistical computations. Table III gives the results computed from elevation errors for the three DEMs: the linear errors with 68% and 90% levels of confidence (LE68 and LE90, respectively), the bias and the percentage of class over three times LE68 (in meters).

Table III: Statistical results (in meters) from the comparison of each stereo DEM (SPOT, EROS, IKONOS and QuickBird) with the LIDAR elevation data: the linear errors with 68% and 90% level of confidence (LE68 and LE90, respectively), the bias and the percentage of the class over three times LE68.

Stereo-Sensors	LE68	LE90	Bias	Over three LE68
SPOT-5	6.5 m	10 m	2 m	0.7%
EROS-A	20 m	31 m	3 m	3.7%
IKONOS	6.4 m	10 m	6 m	0.1%
QuickBird	6.7 m	9 m	6 m	0.6%

The general results for SPOT, EROS, IKONOS and QuickBird (LE68 of 6.5, 20, 6.4, and 6.7 m) are respectively, good, poor and medium when compared to the stereo-bundle adjustment RMS *Z*-residuals (Table II), but also in relation with the pixel for each stereo-image (5, 1.8–2.5, 1, and 0.61 m, respectively) combined with *B/H* of 0.77 for SPOT, 0.7 for EROS, 1 for IKONOS and 1.1 for QuickBird. For EROS the 20-m LE68 errors were mainly due to the same problems previously mentioned for the mismatched areas. In order to confirm this hypothesis, the DEM was cut into four horizontal parts according to the matching score results (Fig. 8). New elevation statistics were computed for each horizontal part, and LE68 of 45, 10, 15, and 10 m from top to bottom were achieved, confirming that better results could then be achieved with EROS-A when pixel spacing of the stereo-images is similar or when the image content is precise and sharp.

For multidate across-track SPOT, LE68 of 6.5 m was achieved, corresponding to an image matching error of ±1 pixel (*B/H* of 0.77), which is similar to previous results generally achieved with different VIR stereo-images (one-pixel image matching accuracy) [20]. The same results (in meters) were achieved with same-date along-track IKONOS (6.4-m LE68) and QuickBird (6.7-m LE68), while its pixel spacing was 1 m and 0.61 m respectively, resulting in a poorer image matching performance (six and tens pixels with *B/H* of 1 and 1.1, respectively). However, these errors were mainly due to canopy/building heights. The largest errors (three times LE68) for SPOT and IKONOS, although representing only a very small percentage, are out of tolerance and cannot be acceptable for DEM in a topographic sense. In order to locate and understand these

largest errors, they were superimposed on the DEMs or the ortho-images. These errors were mainly located in the different shadows (mountain, tree or building). Other large errors (15–20 m) resulted from the elevation comparison of the top of tree versus the ground due to the different spatial resolutions of SPOT, IKONOS, QuickBird and LIDAR data and to the different acquisition seasons. These errors are then specific of the stereo-images (acquired in winter) and the experiment (LIDAR data acquired in summer), but are not representative of the general SPOT/IKONOS/QuickBird stereo-performance for DEM generation.

In fact, these DEMs stereo-extracted from HR data are digital surface models (DSMs), which include the height of natural and human-made surfaces. The more accurate the DEM, the more noticeable are the height of some surfaces and the resulting cartographic features (Figs. 9 and 10). This explains why surfaces and features were not noticeable on the EROS DEM. Consequently, a second elevation accuracy evaluation was performed only on bare surfaces (soils and lakes), where there is no difference between the stereo-extracted elevation and the LIDAR data (Table IV).

Table IV: Statistical results (in meters) from the comparison of DEM generated from stereo SPOT-5, IKONOS and QuickBird data with LIDAR elevation data over bare surfaces (soils and lakes) only: the linear errors with 68% and 90% level of confidence (LE68 and LE90, respectively) and the bias.

Sensors	LE68	LE90	Bias
SPOT-5	2.2 m	5.0 m	-2 m
IKONOS-II	1.5 m	3.5 m	1 m
QuickBird	1.2 m	2.8 m	0 m

The results over bare soil/lakes demonstrate better the real stereo-performance for elevation extraction and DEM generation of SPOT, IKONOS and QuickBird: LE68 of 2.2, 1.5, and 1.2 m, respectively. These results are more consistent with *a priori* 3-D restitution accuracy from the bundle adjustments (around 2 m in *Z*, Table II). Even with a multidate acquisition, SPOT achieved "half-pixel" errors while IKONOS and QuickBird with a same-date acquisition achieved only "1.5-pixel" errors and "two-pixels" errors, respectively: three-to-four time degradation. The first reason could be the use of raw SPOT data (original geometry and radiometry), while IKONOS data were processed as a map-oriented product resulting in a "non-original" geometry and both IKONOS and QuickBird data have a resampled radiometry. A second reason could be the 820-km altitude for SPOT (less orbital perturbations) versus the 500–600-km altitudes for IKONOS and QuickBird.

IV CONCLUSIONS

DEMs were extracted from four different HR stereo images (*B/H* of 0.7, 0.77, 1, and 1.1 for SPOT, EROS, IKONOS and QuickBird, respectively) using the 3-D CCRS physical

geometric model and multi-scale image matching: across-track multidate SPOT-5 (5 m) and in-track same-date EROS-A (1.8 m), IKONOS-II (0.8 m), and QuickBird (0.61 m). These images were acquired over a hilly residential/rural area in Québec, Canada. The stereo-bundle adjustments of geometric models using 10–18 GCPs enabled *a priori* 3-D restitution accuracy, which includes feature extraction error, to be estimated (around 2–5 m in the three axes). However, the internal accuracy of stereo-models is better, in the order of one pixel or less depending upon the sensor. The stereo-extracted DEMs, using a multiscale cross-correlation method, were then compared to accurate elevation LIDAR data, and LE68 of 6.5, 20, 6.4, and 6.7 m were obtained for SPOT, EROS, IKONOS and QuickBird, respectively. The poor results for EROS were due to the combinations of two factors, differences of pixel spacing in the stereo-images and the forest coverage, which induced errors in the image matching process. Better results (10-m LE68) were obtained when one of these factors was not present. For SPOT, IKONOS and QuickBird, the largest errors (over three times LE68) occurred in the shadowing areas of mountains, trees, and/or buildings. In addition, errors were due to the elevation comparison between winter-acquired stereo-images (no leaves in deciduous trees) and summer-acquired LIDAR data (leaves in deciduous trees). Since the surface heights were included in terrain elevation and its evaluation, elevation errors were thus evaluated on bare surfaces (soils and lakes), where there is no elevation difference between the stereo DEMs and the LIDAR data. The results (1.2–2.2-m LE68) over bare surfaces are a good indication of the general SPOT, IKONOS and QuickBird stereo-performance for DEM generation. However, multidate SPOT (raw data, high orbit, *B/H* of 0.77) achieved better results than same-date IKONOS or QuickBird (preprocessed data, low orbit, *B/H* of around one): 0.5 pixel versus 1–2 pixels.

Acknowledgements

The author would like to thank D. Giacobbo and SPOT-Image for the SPOT data, R. Hellerman and ImageSat International for the EROS data, R. Matte (*Ministère des Ressources naturelles du Québec*, Canada) for the topographic data, GPR Consultants (Québec, Canada) for the LIDAR survey, the two anonymous reviewers, A. Chichagov and K. Naluzny (CCRS, NRCan) for reviewing and improving the manuscript, R. Chénier (Consultants TGIS, Incorporated, Canada), and S. Grassi (Università degli Studi di Perugia, Italy) for data processing.

References

[1] V. Kaufmann und W. Sulzer, "Über die Nutzungsmöglichkeit hochauflösender amerikanischer Spionage-Satellitenbilder (1960-1972)," *Vermessung und Geoinformation*, Heft 3/97, pp.166-173, 1997.

[2] G. Konecny, "Mapping from Space," in *Remote Sensing for Environmental Data in Albania: A Strategy for Integrated Management*, *Tirana, Albania.* NATO Science Series, M. F. Buchroithner, Ed. Dordrecht, The Netherlands: Kluwer, 2000, vol. 72, pp. 41-58.

[3] L. W. Fritz, "The Era of Commercial Earth Observation Satellites," *Photogramm. Eng. Remote Sens.*, vol. 62, no. 1, pp. 39-45, 1996.

[4] A. Bouillon, E. Breton, F. de Lussy, and R. Gachet, "SPOT5 HRG and HRS first in-flight geometric quality results," in *Proc. SPIE Conf. Sensors, System, Next Generation Satellites VII,* Vol. 4881A, Agia Pelagia, Crete, Greece, Sept. 22-27, 2002, Paper 4881A-31.

[5] Th. Toutin, "Elevation modeling from satellite data," *Encyclopedia of Analytical Chemistry: Applications, Theory and Instrumentation,* R. A. Meyers, Ed., Chichester, U.K.: Wiley, 2000, vol. 10, pp. 8543-8572. Online. [Avalaible]: http://www.ccrs.nrcan.gc.ca/ccrs/rd/sci_pub/bibpdf/4622.pdf.

[6] F. Leberl, "Radargrammetry," *Manual of Remote Sensing,* F. M. Henderson and A. J. Lewis, Eds. New York, Wiley: 1998, pp. 183-269.

[7] S. N. Madsen and H. A. Zebker, "Imaging radar interferometry," *Manual of Remote Sensing,* F. M. Henderson and A. J. Lewis, Eds. New York: Wiley, 1998, pp. 359-380.

[8] H. M. Ridley, P. M. Atkinson, P. Aplin, J.-P. Muller and I. Dowman, "Evaluating the Potential of the Forthcoming Commercial U.S. High-Resolution Satellite Sensor Imagery at the Ordnance Survey®," *Photogramm. Eng. Remote Sens.*, vol. 63, no. 8, pp. 997-1005, 97.

[9] R. Li, "Potential of High-Resolution Satellite Imagery for National Mapping Products," *Photogramm. Eng. Remote Sens.*, vol. 64, no. 12, pp.1165-1170, 1998.

[10] Th. Toutin, "DTM generation from Ikonos in-track stereo images using a 3D physical model," *Photogramm. Eng. Remote Sens.*, vol. 70, no. 6, pp. 695-702, 2004. Online. [Available]: http://www.ccrs.nrcan.gc.ca/ccrs/rd/sci_pub/bibpdf/13291.pdf

[11] J.-P. Muller, J.-R. Kim, and L. Tong, "Automated mapping of surface roughness and landuse from simulated and spaceborne 1m data," in *Automatic Extraction of Man-Made Objects From Aerial and Space Images (III),* E. P. Baltsavias, A. Gruen and L. van Gool, Eds: A.A. Balkema, 2001, pp. 369-379.

[12] K. Di, R. Ma, and R. Li, "Geometric Processing of Ikonos Stereo Imagery for Coastal Mapping Applications," *Photogramm. Eng. Remote Sens.*, vol. 69, no. 8, pp.873-879, 2003

[13] Th. Toutin and Ph. Cheng, "QuickBird: a milestone for high resolution mapping," *Earth Observation Magazine*, vol. 11, no. 4, pp. 14-18, 2002. Online. [Avalaible]: http://www.ccrs.nrcan.gc.ca/ccrs/rd/sci_pub/bibpdf/13212.pdf.

[14] Th. Toutin, "Error tracking in IKONOS geometric processing using a 3D parametric modelling," *Photogramm. Eng. Remote Sens.*, vol. 69, no. 1, pp. 43-51, 2003. Online. [Avalaible]: http://www.ccrs.nrcan.gc.ca/ccrs/rd/sci_pub/bibpdf/13102.pdf.

[15] G. Dial, "IKONOS Satellite Mapping Accuracy," in *Proc. ASPRS Congress*, Washington DC, May 26, 2000.

[16] L.-C. Chen and Teo, T.-A., "Rigorous Generation of Orthophotos from EROS-A High Resolution Satellite Images," in *Proc. International Archives of Photogrametry and Remote Sensing and Spatial Information Sciences*, vol. 34 (B4), Ottawa, ON, Canada, July 8-12, 2002, pp. 620-625.

[17] Robertson, B., "Rigorous Geometric Modeling and Correction of QuickBird Imagery, " in *Proc. IGARSS*, Toulouse, France, July 21-25, 2003.

[18] R.A. Fowler, "The Thorny Problem of LIDAR Specifications," *Earth Observation Magazine*, vol. 10, no. 4. pp. 13-17, 2001. Online. [Available]: http://www.lasermap.com/laserM/english/princ.htm.

[19] E. Mikhail and F. Ackermann, *Observations and Least Squares*, New York: Harper & Row, 1976, p. 497.

[20] E. Gülch, "Results of Test on Image Matching of ISPRS WG III/4," *ISPRS J. Photogramm. Remote Sens.*, vol. 46, no. 1, pp. 1-8, 1991.